Journal of Fluids and Structures 17 (2003) 875–885

JOURNAL OF FLUIDS AND STRUCTURES

www.elsevier.nl/locate/jnlabr/yjfls

Elasto-dynamics of multihulls in nonlinear beam seas—a multibody–BEM approach

R. Kral, E. Kreuzer*, V. Schlegel

Mechanics and Ocean Engineering, Technical University Hamburg-Harburg, Hamburg 21071, Germany

Received 20 January 1999; accepted 13 January 2003

Abstract

Many floating structures in naval architecture and ocean engineering cannot be modelled as a single rigid body. Even for ships, models of interconnected bodies may be necessary for an adequate description of the dynamics. The dynamic behavior of these floating structures is significantly influenced by fluid–structure interactions. So far, most available methods for analyzing these interactions are restricted to single bodies, small wave amplitudes and small body motions, or both. In the present paper, a two-dimensional boundary integral approach with fully nonlinear boundary conditions on the free surface is used to investigate the dynamic behavior of catamarans in nonlinear beam seas. In the model introduced here, the two hulls of a catamaran are connected by elastic beams. Beams and hulls are modelled as multibody systems. The results of numerical simulations are shown for selected configurations.

1. Introduction

Fast catamaran ferries are rapidly becoming important as means of transportation. Since such ferries cross open waters, sea keeping considerations are important. In this paper, we investigate the influence of the elasticity of the coupling between the hulls on the motion of the bihull–beam system. The connecting beams are modeled as a chain of rigid beams with rotational springs and dashpots in the joints in order to represent stiffness and damping.

The dynamic behavior of floating bodies is significantly influenced by fluid–structure interaction between the bodies and the fluid. Hence, in addition to the differential equation of motion of the dry system the governing equations of the fluid must be solved. For a single floating body results can be found in the literature, e.g., Cointe et al. (1990), Tanaka and Nakamura (1993), van Daalen (1993), and Haack (1996).

Only few of the programs described in these references have been designed to handle more than one floating body. Rigid connections between the bodies or connections that do not reduce the number of degrees of freedom, e.g., ideal (massless) springs, are relatively easy to implement. If the connection between the bodies constrains the motion, the dynamics of the structure are more difficult to describe, Kral and Kreuzer (1999). Additional effort is necessary to discretize continuous elastic elements with distributed mass.

The numerical treatment of the problem considered here requires an efficient computation scheme for the solution of the flow problem. Compared with other methods the direct boundary-element method (BEM) offers several advantages for this specific application for the following reasons.

(i) All quantities of interest—either given or unknown—are located on the boundary itself (see problem formulation).

*Corresponding author.
E-mail address: kreuzer@tu-harburg.de (E. Kreuzer).

0889-9746/03/$ - see front matter
doi:10.1016/S0889-9746(03)00012-4

(ii) In general large, arbitrarily shaped domains have to be considered for practical purposes; this causes large discretization expenses for other methods (e.g., finite elements or finite differences). Since only nodes on the boundaries have to be considered, large deformations are easier to handle with BEM.

(iii) High curvatures arise when the discrete model of the geometry is formulated, especially on the free surface and where the free surface meets floating bodies. With the fully Lagrangian BEM formulation, the density of nodes increases in regions of high curvatures.

(iv) Only the wetted parts of the surfaces of the structures have to be taken into account, in order to adapt the method to fixed or floating structures. Even large body movements will not require a remeshing in the fluid domain. Finite element methods will cause remeshing in this region due to element distortion or moving grids. Finite volume methods combined with a volume of fluid interface model will not require remeshing either, but these methods tend to spread the interface between two fluids or fluids and solids over a number of cells.

(v) The time-dependent pressure distribution on the wetted surfaces is easily available for the force and moment loading of the structures. With indirect methods, e.g. the panel method, the pressure has to be calculated from source strengths. For finite element and finite volume methods pressure distribution is available as part of the solution, too.

2. Problem formulation

All real fluids are viscous and compressible. To simplify the model, we ignore less important effects. In order to solve the fluid flow problem usual assumptions of incompressibility and irrotational flow are made, Newman (1977). These assumptions are justified for the following reasons. Floating bodies moving mainly with the waves cause negligible or no separation near the corners of the bodies, hence, viscosity has little effect on the flow. The compressibility of water is very small, therefore, the density of the fluid is not changed within the range of expected pressure differences.

The discussed simplifications allow to introduce the potential flow concept, described by Laplace's equation

$$\operatorname{div} \boldsymbol{u} = \operatorname{div} \operatorname{grad}\ \Phi = \nabla^2 \Phi = 0, \tag{1}$$

where $\boldsymbol{u}$ is the fluid velocity and Φ the corresponding velocity potential. The equation of motion of the fluid particles can be reduced to Bernoulli's equation

$$\frac{\mathrm{D}\Phi}{\mathrm{D}t} = -gy - \frac{1}{\rho}p - \frac{|\boldsymbol{u}|^2}{2} + \boldsymbol{v}^{\mathrm{T}}\boldsymbol{u}, \tag{2}$$

where g is the gravitational acceleration, y is the vertical position of the considered point, ρ is the density of the fluid, and the pressure is p. In this formulation we must distinguish between the velocity vector of a fluid particle $\boldsymbol{u}$ and the velocity vector $\boldsymbol{v}$ of a point moving relative to the fluid. A schematic representation of the numerical model is shown in Fig. 1.

The flow problem can be solved by transforming Laplace's equation, following Brebbia et al. (1984), into an integral equation of the form

$$C(\boldsymbol{x})\Phi(\boldsymbol{x}) = \int_{\Gamma} u_n(\xi) G(\boldsymbol{x}, \xi)\, \mathrm{d}\gamma(\xi) - \int_{\Gamma} \Phi(\xi) \frac{\partial G(\boldsymbol{x}, \xi)}{\partial \boldsymbol{n}(\xi)}\, \mathrm{d}\gamma(\xi). \tag{3}$$

Here, Γ is the boundary of the considered domain Ω, C is a geometry-dependent constant, G the fundamental solution of the problem, i.e., $G = 1/2\pi \ln(1/|\boldsymbol{x} - \xi|)$ in two dimensions, Φ again the velocity potential, $u_n = \partial \Phi/\partial n$ is the

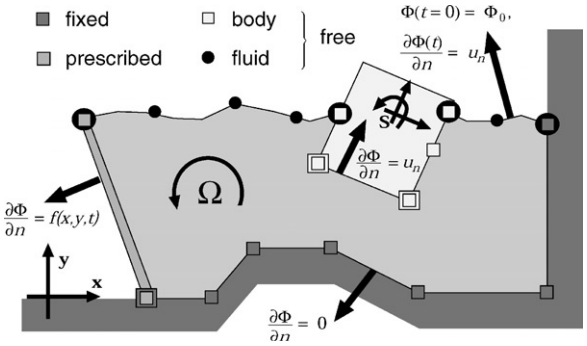

Fig. 1. Discretization and boundary conditions.

component of the velocity vector in the normal direction at the boundary, and $\boldsymbol{x}$ and $\boldsymbol{\xi}$ denote the position vectors for field and source points, respectively.

The integral equation (3) provides one equation per field point or node $\boldsymbol{x}$. If either the normal velocity $u_n(\boldsymbol{x})$ or the velocity potential $\Phi(\boldsymbol{x})$ is known on every part of the boundary, a system of linear equations can be obtained. If Ω is discretized by a direct boundary element approach, we obtain the approximation

$$(\boldsymbol{C}+\boldsymbol{H})\tilde{\Phi}(\boldsymbol{x})=\boldsymbol{F}\tilde{\boldsymbol{u}}_n(\boldsymbol{x}), \tag{4}$$

where the vectors $\tilde{\Phi}$ and $\tilde{\boldsymbol{u}}_n$ consist of the nodal values. The matrices $\boldsymbol{C}$, $\boldsymbol{H}$, and $\boldsymbol{F}$ are defined by

$$\begin{aligned}
&\boldsymbol{C}=[C_{ij}],\\
&\boldsymbol{H}=\left[\int_\Gamma \varphi_i(\boldsymbol{\xi})\frac{\partial G(\boldsymbol{x}_j,\boldsymbol{\xi})}{\partial \boldsymbol{n}(\boldsymbol{\xi})}\,\mathrm{d}\gamma(\boldsymbol{\xi})\right], \quad i=1,\ldots,n_\varphi,\\
&\boldsymbol{F}=\left[\int_\Gamma \varphi_i(\boldsymbol{\xi})G(\boldsymbol{x}_j,\boldsymbol{\xi})\,\mathrm{d}\gamma(\boldsymbol{\xi})\right], \quad j=1,\ldots,n_q,
\end{aligned} \tag{5}$$

where n_φ depends on the order of the shape functions φ_i of the elements (linear, quadratic, splines, etc.), and n_q is the number of nodes. Normally, the number of global shape functions n_φ equals the number of nodes n_q.

To develop a mixed boundary value problem, the known and the unknown boundary conditions in Eq. (4) have to be rearranged into a set of linear equations

$$\boldsymbol{A}\boldsymbol{y}=\boldsymbol{b}. \tag{6}$$

Here, $\boldsymbol{A}$ is a dense and non-symmetric matrix, in general. The right-hand side $\boldsymbol{b}$ of Eq. (6) is given by the following boundary conditions (see Fig. 1):

(a) at impermeable fixed boundaries, e.g., the bottom or walls of a wave tank, the velocity component in the normal direction to the boundary vanishes, i.e., $u_n=0$;

(b) at impermeable moving boundaries the motion, i.e., normal velocity, is prescribed by a function f in space and time by $u_n=f(x,y,t)$; this type of boundary is needed to describe features such as wave makers;

(c) at the impermeable boundaries of the submerged parts of free floating rigid bodies the time-dependent normal velocity is given by the normal direction of the time derivative of the nodal position $u_n=(\mathrm{d}\boldsymbol{r}/\mathrm{d}t)\boldsymbol{n}$, and is calculated from the equations of motion of the rigid body;

(d) the free surfaces of the fluid are described by the fluid particles themselves. At these boundaries, the time-dependent velocity potential $\Phi(t)$ is given; thus, the normal velocity of a fluid particle can be written $u_n=\partial\Phi(t)/\partial\boldsymbol{n}$, and is part of the boundary element solution.

On the impermeable boundaries (a)–(c) the normal velocity u_n is known. As there is no flow through these boundaries, the normal velocity relative to these boundaries must vanish. The nodes in the discrete model are, therefore, free to move parallel to the boundary but not normal to it. In order to determine the time-dependent boundary conditions (c) and (d), an additional initial value problem has to be set up and solved. The motion of the fluid particles at the free surfaces is described by a Lagrangian formulation, with $\boldsymbol{v}$ set equal to $\boldsymbol{u}$ in Eq. (2). The equations of motion for the fluid particles yield in fully nonlinear form

$$\begin{aligned}
&\frac{\mathrm{D}\boldsymbol{x}_{fl}}{\mathrm{D}t}=\nabla\Phi=\boldsymbol{u},\\
&\frac{\mathrm{D}\Phi}{\mathrm{D}t}=-gy-\frac{1}{\varrho}p+\frac{|\boldsymbol{u}|^2}{2}.
\end{aligned} \tag{7}$$

Here, $\boldsymbol{x}_{fl}=[x_{fl}\ \ y_{fl}]^{\mathrm{T}}$ denotes the position vector of the fluid particles on the free surface, and $p=p_{\mathrm{amb}}$ the pressure on the free surface. The initial condition is given by $\Phi(t=0)=\Phi_0$.

Kral et al. (1997) have shown that even for moderate forcing amplitudes nonlinearities have to be taken into account.

The positions and velocities of the floating bodies are known in every time step, they are part of the boundary conditions, whereas the pressure distribution on the wetted surface, i.e., the acceleration, is part of the solution. The potential flow problem is solved for a known set of state variables of the multibody system, and the solution of the flow field provides forcing vectors for the equation of motion of the multibody system. Since the flow field does not depend (at least not directly) on the acceleration of the floating bodies, the differential equations of the multibody system can be solved after the boundary integral equations have been solved. Nevertheless, the differential equations of both subsystems have to be integrated simultaneously with respect to time.

In long-crested beam seas the forward speed has no effect on the wave excitation, therefore, a two-dimensional model is sufficiently accurate to analyze the dynamics. Bow and stern influences are neglected in the model.

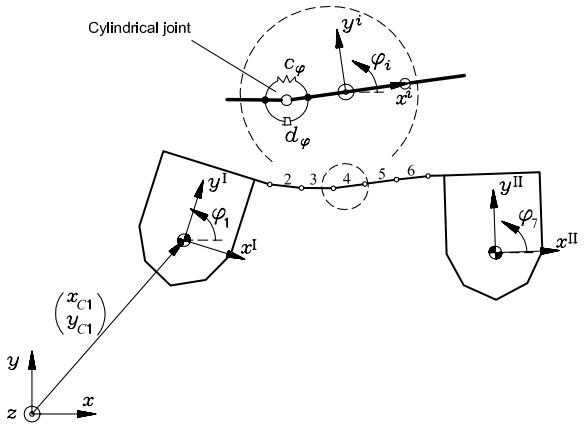

Fig. 2. Reference frames of the multibody system.

The coupling beams of the catamaran have been modeled as a chain of seven rigid bodies coupled by hinges (cylindrical joints) are constrained by rotational springs and dashpots. Bockstedte (1998) investigated different discretizations for the elastic beams. It was found by investigating several models of the coupling beams that seven discrete links are sufficient for the considered configuration and frequency range[1] to get an accurate representation of the continuous elastic beam. The relative error of the first natural frequency of the seven link model compared to the continuous beam is less than 2.5 percent. The first eigenmodes of the discrete model resemble those of the continuous model very well.

The generalized coordinates of the discrete model shown in Fig. 2 are

$$\boldsymbol{z}_1 = [x_{\mathrm{C1}}\ y_{\mathrm{C1}}\ \varphi_1\ \varphi_2\ \varphi_3\ \varphi_4\ \varphi_5\ \varphi_6\ \varphi_7]^{\mathrm{T}} \tag{8}$$

with respect to the centers of mass of the first hull. All angles φ_i $(i = 1, 7)$ are measured from the horizontal plane in the positive sense. In state space representation, $\boldsymbol{z}_2$ is the time derivative of $\boldsymbol{z}_1$, i.e., $\boldsymbol{z}_2 = \dot{\boldsymbol{z}}_1$:

$$\boldsymbol{z}_2 = [\dot{x}_{\mathrm{C1}}\ \dot{y}_{\mathrm{C1}}\ \dot{\varphi}_1\ \dot{\varphi}_2\ \dot{\varphi}_3\ \dot{\varphi}_4\ \dot{\varphi}_5\ \dot{\varphi}_6\ \dot{\varphi}_7]^{\mathrm{T}}. \tag{9}$$

The reference frames used to describe the positions of the coupling elements are shown in Fig. 2. The initial values are

$$\boldsymbol{z}_1(t=0) = [x_{\mathrm{C10}}\ y_{\mathrm{C10}}\ \varphi_{10}\ \varphi_{20}\ \varphi_{30}\ \varphi_{40}\ \varphi_{50}\ \varphi_{60}\ \varphi_{70}]^{\mathrm{T}} \tag{10}$$

and

$$\boldsymbol{z}_2(t=0) = [\dot{x}_{\mathrm{C10}}\ \dot{y}_{\mathrm{C10}}\ \dot{\varphi}_{10}\ \dot{\varphi}_{20}\ \dot{\varphi}_{30}\ \dot{\varphi}_{40}\ \dot{\varphi}_{50}\ \dot{\varphi}_{60}\ \dot{\varphi}_{70}]^{\mathrm{T}}. \tag{11}$$

The equations of motion were generated with the help of the multibody system program NEWEUL (Kreuzer and Schiehlen, 1990). The equations of motion of the rigid bodies can be formulated in the state space as follows:

$$\frac{\mathrm{d}}{\mathrm{d}t}\underbrace{\begin{bmatrix}\boldsymbol{z}_1\\ \hline \boldsymbol{z}_2\end{bmatrix}}_{\boldsymbol{z}} = \underbrace{\left[\begin{array}{c|c}\boldsymbol{0} & \boldsymbol{I}\\ \hline \boldsymbol{A}_1 & \boldsymbol{A}_2\end{array}\right]}_{\boldsymbol{A}}\underbrace{\begin{bmatrix}\boldsymbol{z}_1\\ \hline \boldsymbol{z}_2\end{bmatrix}}_{\boldsymbol{z}} + \underbrace{\begin{bmatrix}\boldsymbol{0}\\ \hline \boldsymbol{M}^{-1}\boldsymbol{h}\end{bmatrix}}_{\boldsymbol{b}}, \tag{12}$$

where $\boldsymbol{z}$ denotes the vector of state variables, $\boldsymbol{I}$ is the identity matrix and $\boldsymbol{M}$ the mass matrix. The sub-matrix $\boldsymbol{A}_1 = -\boldsymbol{M}^{-1}(\boldsymbol{K}+\boldsymbol{N})$ contains the conservative and non-conservative forces, while $\boldsymbol{A}_2 = -\boldsymbol{M}^{-1}(\boldsymbol{D}+\boldsymbol{G})$ accounts for the damping and gyroscopic forces. The vector $\boldsymbol{h}(t)$ describes the excitation, which includes the external forces $\boldsymbol{f}_e$ and the external torques $\boldsymbol{t}_e$. They are calculated from the time-dependent pressure distribution $p(t)$ on the wetted surfaces of

[1] For the parameters given below the first natural frequencies of the beam are 4.3, 11.8, and 23.8 Hz, whereas the forcing frequencies are of the order of 1 Hz.

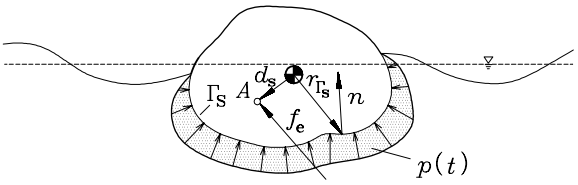

Fig. 3. Excitation forces.

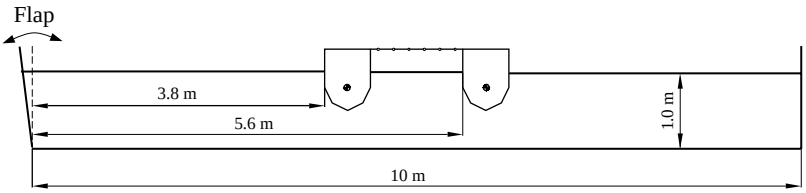

Fig. 4. Initial position in the numerical wave tank.

the floating bodies (see Fig. 3) as follows:

$$\boldsymbol{f}_e = \int_{\Gamma_{\text{sub}}} p(t)\boldsymbol{n}\,\mathrm{d}\gamma, \tag{13}$$

$$\boldsymbol{t}_e = \boldsymbol{d}_s \times \boldsymbol{f}_e, \tag{14}$$

where $\boldsymbol{n}$ is the outward unit normal vector and $\boldsymbol{d}_s$ is the distance vector from the center of mass to the center of buoyancy of the floating body. The unknown time-dependent pressure on the submerged surface is obtained by transforming (2) into

$$p(t) = \rho\left(-gy - \frac{|\boldsymbol{u}|^2}{2} - \frac{\mathrm{D}\Phi}{\mathrm{D}t} + \boldsymbol{v}^{\mathrm{T}}\boldsymbol{u}\right). \tag{15}$$

The time derivative $\mathrm{D}\Phi/\mathrm{D}t$ can be approximated numerically, if the nodal values $\tilde{\Phi}$ of the previous time step (or steps) have been stored.

The numerical implementation of this approach (Haack et al., 1991; Haack, 1996) uses cubic spline-elements on the free surface in order to approximate the extreme curvature of nonlinear gravity waves and to compute the tangential derivatives in addition to the normal derivatives. The normal direction does not change continuously where the free surface meets floating structures or walls of the tank. These points are modelled by means of the double nodes. Haack (1996) studied the convergence of the method and compared calculated pressures on the wave-maker to measured data. The agreement of the numerical and experimental results was excellent.

3. Results

We intended to verify the simulations we present in this paper experimentally, therefore, all calculations of this paper are based on a two-dimensional mathematical representation of the wave tank in the laboratory of the department of Mechanics and Ocean Engineering of the Technical University Hamburg-Harburg. The parameters of the idealized catamaran model were chosen to match a model we can use for experiments in the laboratory. The tank is equipped with a flap type-wave maker as sketched in Fig. 4.

In order to simulate the dynamic behavior, we have to solve a (numerical) initial value problem. Hence, we have to prescribe initial conditions or values. All simulations start with initial conditions set to zero, because nonzero initial conditions on the free surface are difficult to prescribe. In this case a set of nodal positions, potential values, and velocities, which are solutions of the differential equation, i.e., a restart of a previous simulation, would be required.

The simulation is based on an idealized catamaran model, Fig. 5. The mass of the floating bodies is $m_{\text{hull}} = 237.3$ kg, the moment of inertia is $I_{\text{hull}} = 20$ kg m^2 with respect to the centroid. The parameters of the connection between the hulls have been chosen to simulate a polypropylene plate of 5 mm thickness. The plate has a mass per section of $m_{\text{link}} = 0.9$ kg and a length of $l_{\text{link}} = 0.2$ m. The rotational springs have a stiffness of $c_\varphi = 67.71$ N m; the damping coefficient is $d_\varphi = 0.1$ N m s. The amount of damping is in the order of the expected material damping. Damping has a

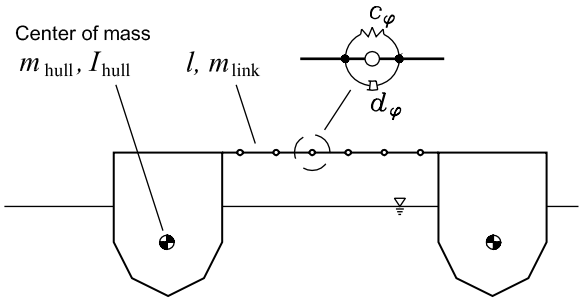

Fig. 5. Parameters of the system

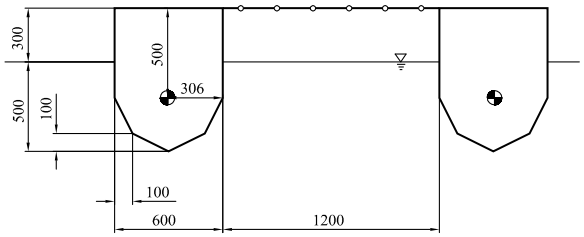

Fig. 6. Geometry of the hulls.

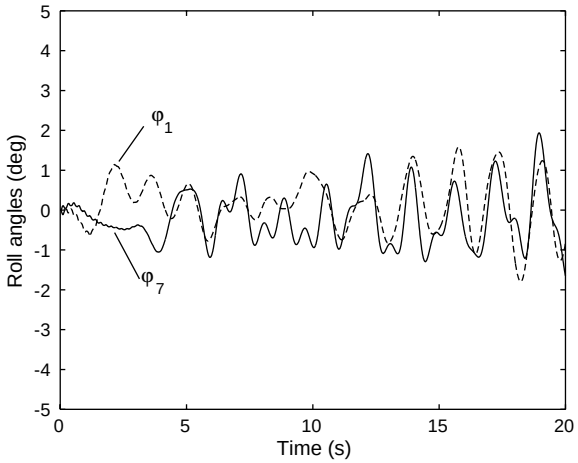

Fig. 7. Roll motion of the hulls for a flap frequency of 1.2 Hz.

stabilizing effect on the simulation. The cross-section of the two symmetric bodies is a simplified hull cross-section of a twin-hull. Their geometry is given in Fig. 6.

The weight of the beam causes a roll moment with respect to the center of gravity of the hulls. To compensate for this roll moment the center of mass of the hulls was moved 6 mm outwards from the center of buoyancy. Since the simulation starts with a straight beam, which is not the equilibrium position, free vibrations starting with an initial deflection of the beam are observed (e.g. Fig. 7). The beam vibrations cause the small ripples that can be seen in the plots of the roll angles of the hulls.

The dynamic behavior of the floating multibody system has been simulated for flap frequencies from 0.6 to 1.2 Hz. Since the simulation uses fully reflecting boundary conditions on the far end, the energy in the tank is increasing as long as the flap is moving. To limit the energy input the flap was stopped after 10 s. The roll angles are shown in Figs. 7–11, where φ_1, and φ_7 are the roll angles of the left and right hull, respectively. The angles are measured in the mathematically positive sense from the horizontal plane. The flap amplitude was adjusted to keep the wave height (measured for the second wave train) at about 50 mm.

In the frequency range 0.8–1.0 Hz the roll motion of the hulls is dominated by counter-phase motions of the hulls (see Figs. 8 and 9). At 1.2 Hz, the highest flap frequency, the motion is nearly in phase although there are large differences in the roll amplitudes of the hulls, Fig. 7. For 0.6 Hz, the lowest frequency, the roll motion of the bodies is almost perfectly in phase, Fig. 10. Since this frequency can be identified in the frequency spectrum of the roll motion for all forcing frequencies, 0.6 Hz seems to be close to a natural frequency of the system. The coupling beam is not very stiff here, therefore, the natural roll frequency of a single hull, i.e. about 0.47 Hz, is probably close to a natural frequency of the coupled system. The stiffness of the coupling beam increases the frequency slightly, hence, 0.6 Hz is in the expected range of the natural frequencies.

In Fig. 11 the roll motion of the elastic catamaran is compared with the roll motion of the catamaran with rigid coupling. The wave height was reduced to about 30 mm, since the forcing wave frequency of 0.6 Hz is close to the heave natural frequency of 0.56 Hz of the rigid catamaran. The wavelength at this frequency is about twice the overall width of the model, hence, even for the rigid model significant roll amplitudes are observed.

The wavelengths vary from 1.08 m (1.2 Hz) to about 4.5 m (0.6 Hz). Hence the phase velocity of the waves is 1.30–2.60 m/s. The group velocity is half the phase velocity for deep water, i.e. wavelength up to 2.0 m in this case. The group velocity is approaching the phase velocity for shallow water. The numerical wave tank uses fully reflective boundary conditions of the far end. Based on the group velocities the reflections will reach the floating bodies after 21 s for 1.2 Hz and 10 s for 0.6 Hz. The declining roll angles on the right side of Fig. 10 are caused by reflections that reach the hull with a phase shift.

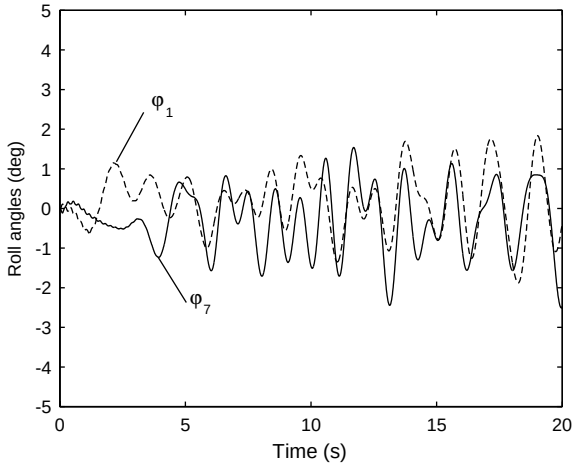

Fig. 8. Roll motion of the hulls for a flap frequency of 1.0 Hz.

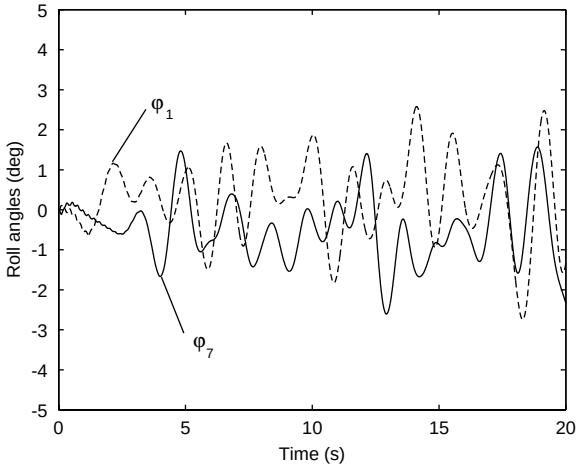

Fig. 9. Roll motion of the hulls for a flap frequency of 0.8 Hz.

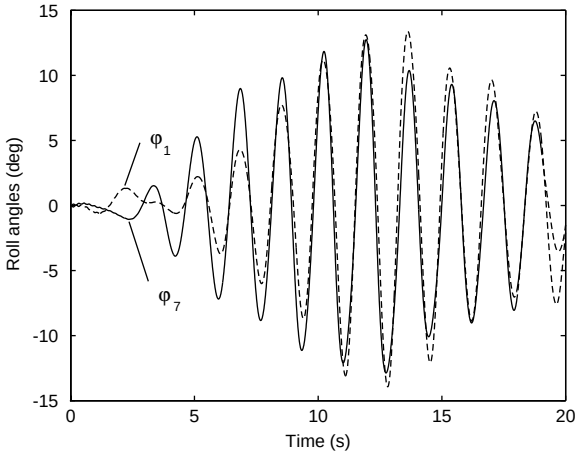

Fig. 10. Roll motion of the hulls for a flap frequency of 0.6 Hz.

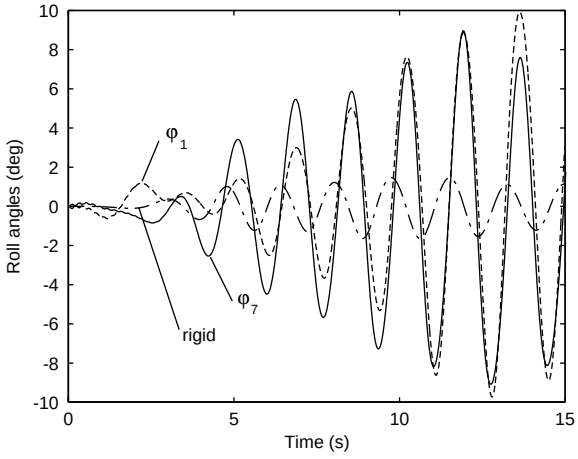

Fig. 11. Roll motion of the elastic catamaran compared with a rigid model, 0.6 Hz, reduced wave height.

The method is not sensitive to changes in the discretization of the fluid boundaries. The submerged parts of the hulls are formed by six straight sections per hull. For the results shown every section has been discretized using cubic elements and nine nodes.

The simulation of the motion of a rigid catamaran was repeated using a finer and a coarser discretization on the wetted part of the hulls, i.e., 13 and 5 nodes, respectively. The relative difference between the finest and coarsest discretization is shown in Fig. 12. The size of the time step was unchanged. The difference of the horizontal positions of the center of gravity is less than 0.45 percent or 127 μm. Since the floating bodies were not restricted by a mooring system, there is no restoring force to the sway motion. Therefore, the differences in the sway motion can increase almost continuously.

It may be noted that irregular frequencies that can cause problems with panel methods in frequency domain are unknown to the direct boundary element approach in time domain based on the fundamental solution used here.

The deformation of the beam can be seen in Figs. 13 and 14, where we have sketched typical deformations of the connecting beam. In these figures a section of the numerical wave tank is shown. Although the hulls are rolling in phase, the beam deformation is much bigger for 0.6 Hz compared with that for 0.8 Hz.

The internal moments in the joints can easily be calculated using the generalized coordinates. In Fig. 15, the bending moments at the joints are plotted. The moment at the ith joint is

$$M_i = c_\varphi(\varphi_{i+1} - \varphi_i) + d_\varphi(\dot{\varphi}_{i+1} - \dot{\varphi}_i). \tag{16}$$

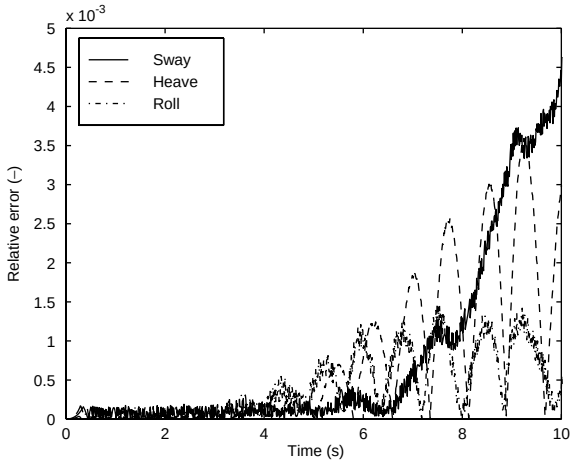

Fig. 12. Relative difference between the coarsest and finest discretization.

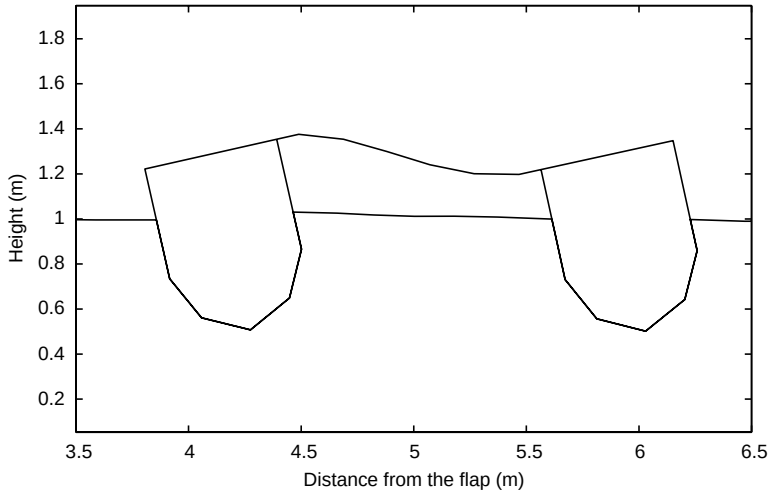

Fig. 13. Deformation of the beam after 12.0 s, flap frequency 0.6 Hz.

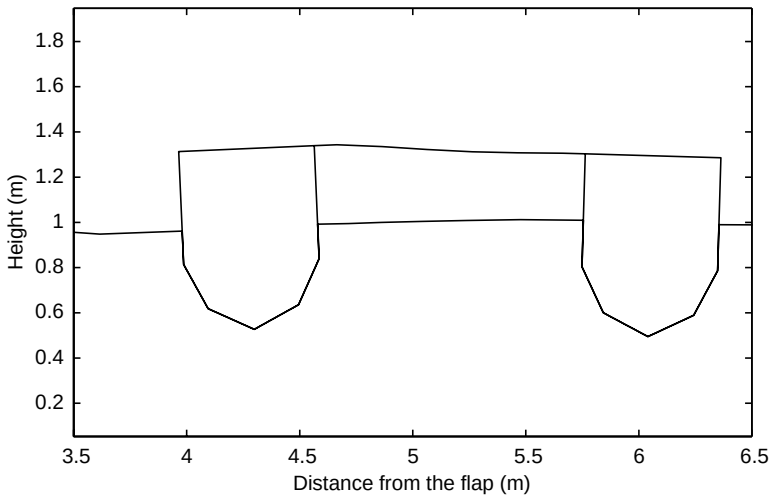

Fig. 14. Deformation of the beam after 14.2 s, flap frequency 0.8 Hz.

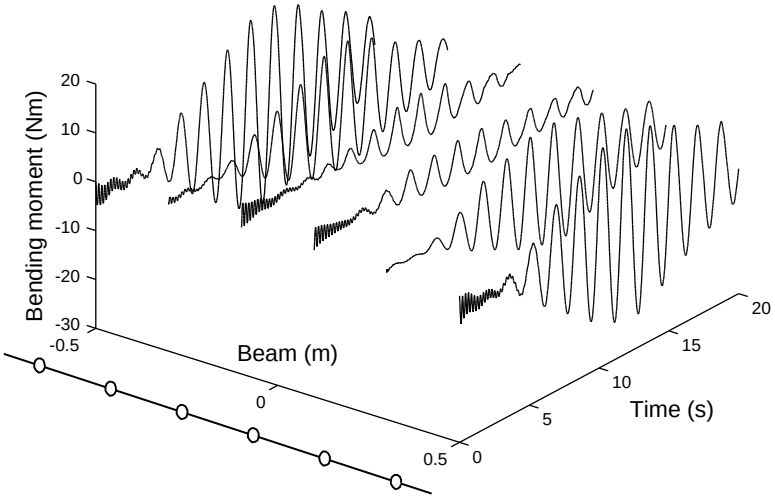

Fig. 15. Internal bending moments, flap frequency 0.6 Hz.

Note that the distance along the beam is measured from the center of the beam. The amplitudes are nearly symmetric with respect to the center-line. The bending moments have opposite signs due to different curvature of the beam at varying positions, see Fig. 15.

All simulations were carried out with a time step $\Delta t = 0.01$ s. About 2 h CPU time are required on a desktop PC (Athlon 900) for 20 s simulation time. For the parameters given above, the lowest natural frequency of the beam is an order of magnitude higher than the natural frequencies of the rigid-body movements of the hulls. If the beam stiffness is increased significantly, the differential equations of the multibody–BEM system will become stiff; the fourth order Adams–Bashforth–Moulton time integrator that is used here limits the range of stable simulations.

4. Conclusions

The dynamic behavior of an idealized twin-hull catamaran in beam seas was simulated for a range of forcing wave frequencies. The elasticity of the beam connecting the hulls of the catamaran has a significant influence on the overall behavior of the system. The multibody system representation of a catamaran is a suitable idealization to analyze the influence of the beam stiffness on the roll motion. Internal loads, e.g., bending moments, can easily be calculated from the generalized coordinates. The reaction forces in the joints would have to be included explicitly in the model to evaluate these forces with other methods than boundary elements plus multibody systems.

The approach described here is not limited to twin-hulls. It can easily be applied to trimarans or other multihulls with an arbitrary number of hulls.

Since seven discrete links are required to get a good representation of the elastic beam between the hulls in the problem considered here, the capacity of the multibody dynamics tool is the limiting factor for the complexity of the model. The (nonlinear) differential equations for a chain of seven rigid bodies are almost impossible to generate without appropriate software tools. The equations of motions as generated by NEWEUL (over 8000 lines) had to be simplified using trigonometric identities and MAPLE to get a minimum of 353 lines of Fortran code.

The fluid dynamics are described by partial differential equations. The equations require integration with respect to space and time. Once the fluid flow has been calculated for the current time step using the boundary element method, the multibody and the fluid dynamics can be integrated with respect to time. Here, the integration of the multibody dynamics part of the presented approach with respect to time is more demanding than that of the fluid dynamics part. The differential equation of the multibody system can become stiff, hence, special integration schemes for stiff equation have to be used. Since the evaluation of the boundary integral equations is rather expensive compared to the equation of motion of the multibody system, a small number of function calls per time step is desirable.

Acknowledgements

The authors would like to thank Andreas Bockstedte, student at the TUHH, whose results are included in Section 3.

References

Bockstedte, A., 1998. Dynamik von Mehrrumpfbooten im Seegang. Student Research Project, Technical University Hamburg-Harburg, Mechanics and Ocean Engineering, Hamburg.

Brebbia, C.A., Telles, J.C.F., Wrobel, L.C., 1984. Boundary Element Techniques. Springer, Berlin.

Cointe, R., Geyer, P., King, B., Molin, B., Tramoni, M., 1990. Nonlinear and linear motions of a rectangular barge in a perfect fluid. In: Proceedings of the 18th Symposium on Naval Hydrodynamics, pp. 85–99.

van Daalen, E., 1993. Numerical and theoretical studies of water waves and floating bodies. Dissertation, University of Twente, Enschede.

Haack, C., 1996. Numerische Analyse der Wechselwirkungen von Schwerewellen und Strukturen—Einsatz der Randelementmethode. Dissertation, VDI-Fortschrittberichte Reihe 7, No. 284, VDI-Verlag, Düsseldorf.

Haack, C., Gravert, P., Schlegel, V., 1991. The modelling of extreme gravity waves: an approach towards a numerical wave channel. In: Proceedings of the First International Conference on Computational Modeling of Free and Moving Boundary Problems, Vol. 1, Fluid Flow, pp. 91–104.

Kral, R., Kreuzer, E., 1999. Multibody systems and fluid-structure interactions with application to offshore structures. In: Multibody System Dynamics, Vol. 3, No. 1, pp. 65–83.

Kral, R., Kreuzer, E., Schlegel, V., 1997. Multibody systems in nonlinear waves. In: Proceedings of the Fourth International Symposium on Fluid–Structure Interaction, Aeroelasticity, Flow-induced Vibration and Noise. ASME, Dallas, pp. 239–245.

Kreuzer, E., Schiehlen, W., 1990. NEWEUL—Software for the generation of symbolical equations of motion. In: Schiehlen, W. (Ed.), Multibody Systems Handbook. Springer, Berlin.

Newman, J.N., 1977. Marine Hydrodynamics. The MIT Press, Cambridge, MA.

Tanaka, Y., Nakamura, T., 1993. Nonlinear simulation model of slow drift oscillation of a floating body with finite amplitude motions. In: Proceedings of the 12th International Conference on Offshore Mechanics and Arctic Engineering, Glassgow, Vol. I, pp. 175–181.